IEEE Photonics Journal
An IEEE Photonics Society Publication

Decenter Error Sensing Technology of Sparse Aperture Telescope Systems

Volume 13, Number 2, April 2021

Yang Liu
Haotong Ma
Bo Qi

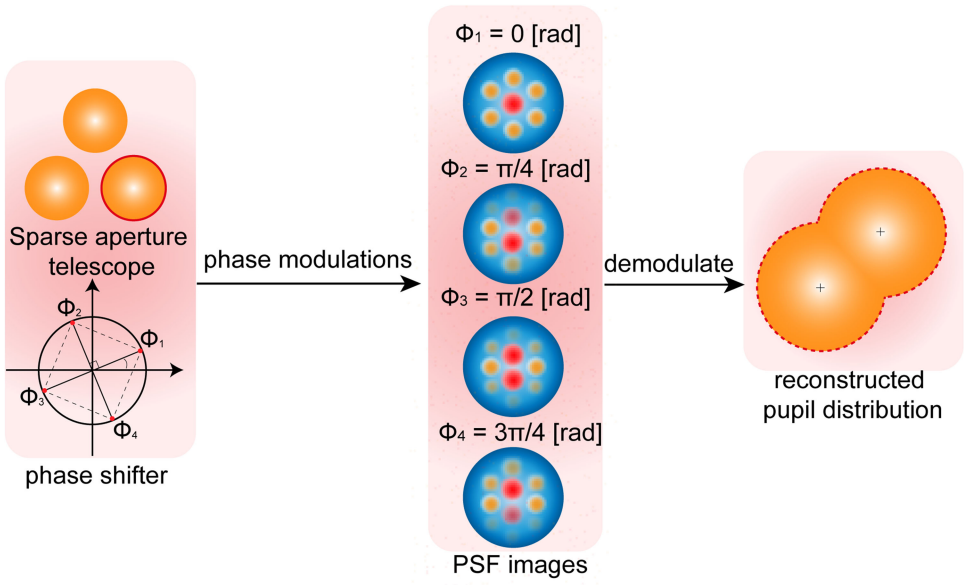

DOI: 10.1109/JPHOT.2021.3064260

Decenter Error Sensing Technology of Sparse Aperture Telescope Systems

Yang Liu, Haotong Ma, and Bo Qi

Key Laboratory of Optical Engineering, Chinese Academy of Sciences, Chengdu 610209, China
Institute of Optics and Electronics, Chinese Academy of Sciences, Chengdu 610209, China
University of Chinese Academy of Sciences, Beijing 100039, China

DOI:10.1109/JPHOT.2021.3064260

Manuscript received January 14, 2021; revised February 22, 2021; accepted March 1, 2021. Date of publication March 8, 2021; date of current version March 26, 2021. Corresponding author: Haotong Ma (e-mail: mahaotong@163.com).

Abstract: The imaging quality of sparse aperture telescope systems is degraded by several factors including design, manufacturing, and arrangement errors. To achieve a high-resolution, the optical system requires an accurate control of not only the wave-front errors such as the piston and tip-tilt but also the decenter errors. Decenter diminishes the field of view of synthetic systems heavily and causes frequency shifting as well. In this paper, we firstly present an approach to sense the decenter of the sparse aperture telescope using the multi-beam interference method based on phase shift and centroid extraction algorithm. The most attractive point of our method is that it can sense not only the decenter but also the other wave-front errors simultaneously, but does not need to install any additional sensors. The numerical simulations are described and preliminary experiments are performed for validation, demonstrating that this technique is efficient and accurate and could be used to guide future sparse aperture telescope error correction.

Index Terms: sparse aperture telescope, decenter sensing.

1. Introduction

With the growing demands for astronomical exploration and distant objects sensing, the present scale of monolithic apertures cannot satisfy the quest for the finer spatial resolution, which makes it an inevitable development trend to manufacture larger telescopes. However, the diameters of such single-aperture systems cannot be enlarged unlimitedly, due to the difficulty of manufacturing large optics and the capacity of launching vehicles. Thus, developing the sparse aperture telescope technology is a great alternative option. Recently, many pioneering works mainly including the segmented mirror telescope and the synthetic aperture telescope have been proposed and validated, such as the James Webb Space Telescope (JWST) [1], the Future Extremely Large Telescope (ELT) [2], and the STAR-9 [3]. These synthetic imaging systems can realize a high-resolution performance that is matched closely to the equivalent monolithic telescopes. The major problem of such synthetic systems is the correction of wave-front errors (WFE), such as piston, tip-tilt, and decenter. To correct these errors and facilitate the application of the synthetic aperture telescopes, many well-known wave-front sensors (WFS) are proposed, such as Shack-Hartmann sensors [8], [9], pyramid sensors [10], dispersed fringe sensors [11], [12] and so on. These sensors are usually used to detect the piston and tip-tilt errors of the sparse aperture systems, but few of them can be applied to sense the decenter of the sub-aperture. To achieve a synthetic image successfully,

there is a well-known Golden Rule [4], [5] needed to be obeyed, that the output pupil of the sparse aperture system to be an exact scaled replica of its entrance pupil [6]. The disproportional mapping generates the decenter in the output pupil plane, which not only decreases the field of view (FOV) of the system but also reduces its image performance [7]. Presently, decenter is corrected through installing edge sensors around each sub-aperture [13]. By measuring the relative heights and gaps of the sub-apertures, edge sensors are able to acquire error data and send commands to the actuators so that the decenters are able to be corrected. These sensors appear on many giant telescopes such as European Extremely Large Telescope [2], Thirty Meter Telescope (TMT) [4] and the Giant Magellan Telescope (GMT) [14]. However, installing additional sensors is costly and makes the system complicated.

In this paper, we firstly propose an approach for decenter sensing in the sparse aperture telescope system using the multi-beam interference method based on phase shift algorithm, inspired from the classical phase-shift interferometry technology (PSIT) [16], [17]. Usually, PSIT is regarded as a WFS and has been utilized to sense the piston and tip-tilt errors [18]. Traditional PSIT requires a set of point spread function (PSF) images formed by the existing sub-apertures and an added small aperture. The added aperture is regarded as a phase shifter to generate phase modulations. Then the reconstructed image is obtained and WFE information is acquired by demodulating those images. But the disadvantage of this method is obvious, that adding another aperture is redundant and makes the compact system complicated. Since that, we have improved this method and directly use one existing sub-aperture as the phase shifter to generate phase modulations. What is more, the decenters of all sub-apertures are extracted in the reconstructed image using the Hough transforms.

Our method for decenter sensing has the following advantages. First, it can sense the decenter directly without installing extra edge sensors, which simplifies the system. Besides that, we can acquire the piston and tip-tilt errors at the same time. Next, we employ a sub-aperture as the phase shifter instead of introducing another one, which makes it feasible for the practical sparse aperture telescope system. The sub-aperture can both be used as the phase shifter and the imaging element. And thirdly, this approach is applicable to both the sparse and the compact telescopes, which means the decenters can be extracted even if the telescope arrays are compact and the reconstructed pupils are overlapped.

The outline of this paper is described as follows. First, in Section 2, we briefly explain the main theory formulas and algorithms about decenter sensing. Then in the Section 3, a numerical simulation intended to extract the decenter errors is briefly described. Next in Section 4, the experiments with a simple configuration are addressed. Finally, Section 5 concludes this paper.

2. Theory

In this section, we introduce the principle of our method associated with the equations and how it works. To begin with, given a sparse aperture telescope with N sub-apertures, a phase modulation Φ_{m} is generated for one sub-aperture, which is regarded as the phase shifter. Then the complex amplitude $A_m(u, v)$ in the exit pupil plane can be written as

$$A_m(u, v) = B_1(u, v)e^{i\phi_m} + \sum_{n=2}^{N} B_n(u, v)e^{ik\Delta_n} \tag{1}$$

where m ranges from 1 to 4, representing that Φ_{m} will further take 4 different values, B_1(u,v) represents the amplitude transmitted by the phase shifter, B_n(u,v) represents the amplitude transmitted by the n^{th} sub-aperture, Δ_n is its unknown WFE, and $k = 2\pi/\lambda$. Then, the optical transfer function (OTF) of this sparse aperture system can be derived

$$OTF_m = FT^{-1}(\left|FT(A_m(u, v))\right|^2) \tag{2}$$

where FT and FT^{-1} stands for the Fourier transform and inverse Fourier transform, respectively. And $|FT(A_m(u,v))|^2$ represents the PSF of the sparse aperture system. Here given (a_n, b_n) as the

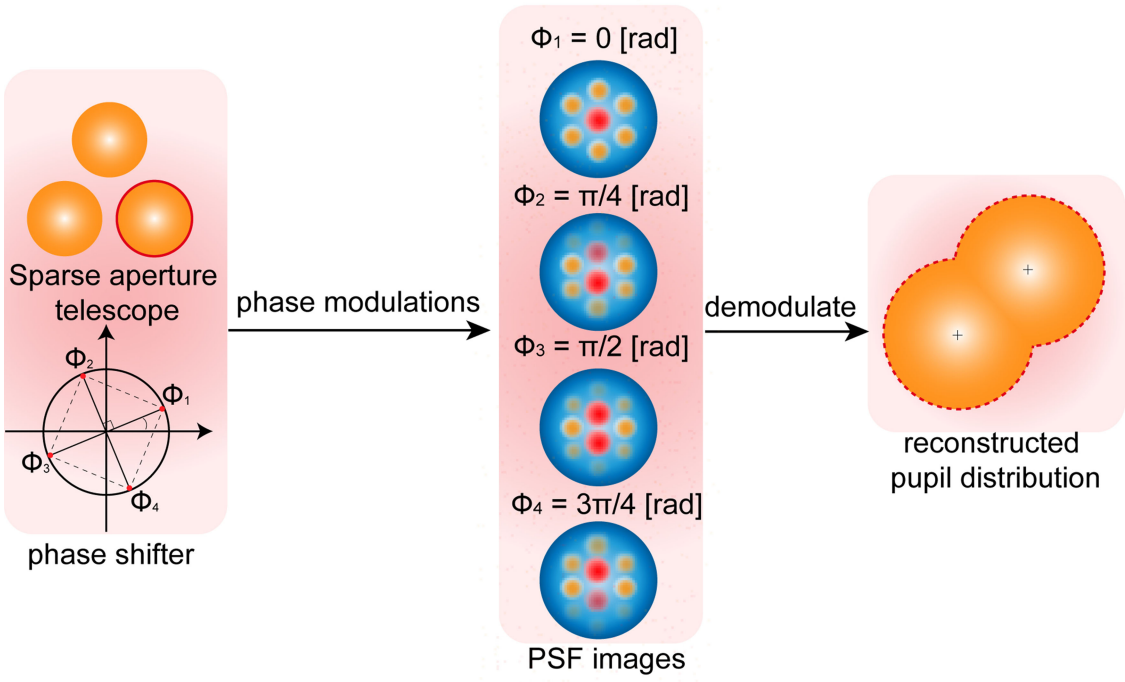

Fig. 1. The schematic of decenter sensing algorithm. Left: the aperture with a red circle is regarded as the phase shifter (introducing 4 phase shifts); middle: 4 PSFs with different phase modulations obtained by the camera; right: reconstructed pupil distribution.

decenter of n^{th} sub-aperture and the phase series $\{0, \pi/2, \pi, 3\pi/2\}$ assigned as the four-time phase modulations, by linearly combining these OTFs, we have a parameter P as

$$P = \frac{1}{4}\sum_{m=1}^{4} OTF_m e^{i\phi_m} = \sum_{n=2}^{N} e^{ik\Delta_n} B_1(u, v) \otimes B_n(u - a_n, v - b_n) \tag{3}$$

Apparently, P is the reconstructed pupil distribution including centering and other WFE information. This step brings a crucial challenge that each sub-aperture is convoluted by the phase shifter, which might cause overlapping among the sub-apertures. Reference [17] indicates that if the size of the phase shifter is greatly smaller than those of the other sub-apertures, the function B_1 can be replaced by the Dirac function and consequently the 3 is able to be simplified. However, introducing a much smaller reference sub-aperture has following disadvantages: (i) it is unpractical to add an extra sub-aperture due to the narrow space and installment complexity of the real sparse aperture system; (ii) the interference effect is difficult to be distinguished due to the big energy difference between the phase shifter and existing sub-apertures. Moreover, the purpose of this paper is to correct the decenter, which is irrelevant with the convolution product in the 3, since the spatial dimension of reference sub-aperture only enlarges the sizes of the other sub-apertures, but does not influence their centering. Thus, we use one of the sub-apertures as the phase shifter to generate the phase modulations instead of adding another smaller one. The Fig. 1 shows how the method works. Based on the reconstructed pupil distribution in eq. (3), we can obtain the decenters of the tested sub-apertures by sensing their centroid positions. To address this issue, a strategy is adopted based on Hough transform algorithm, which is initially proposed by Paul Hough [19] and employed to detect lines in images. Afterwards, many researchers have extended this method to detect arbitrary shapes [20]. The key point of Hough transform is converting the problem of sensing

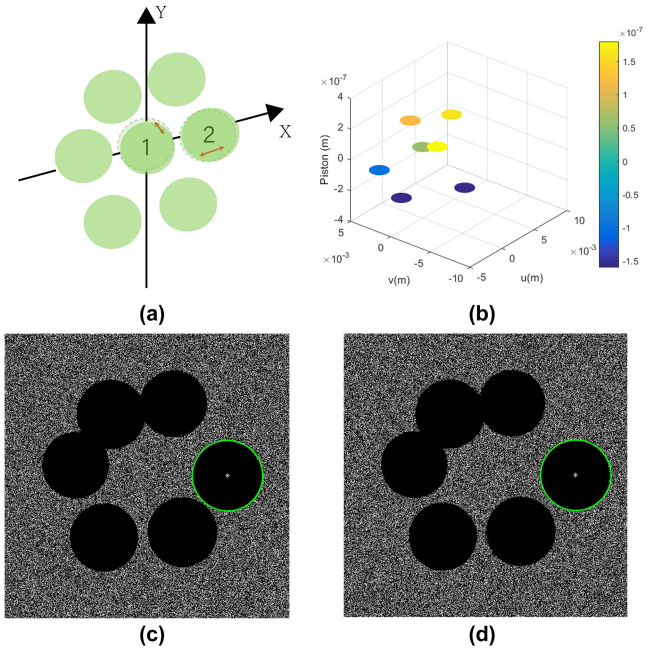

Fig. 2. Simulation setup of a sparse configuration. (a) The seven apertures configuration. Aperture 1 produces phase shifts and aperture 2 produces decenters. (b) The loaded piston errors [−100∼180] nm. (c) The sensing results of Hough transform algorithm at initial position (the target aperture is with green circle). (d) The sensing results of Hough transform algorithm at final position (the target aperture is with green circle).

shape into seeking the maximum of similar featured points. Here, we utilize this method to detect circles (corresponding to the shapes of sub-apertures) so as to extract their centroids.

3. Numerical Simulation

In this section, a numerical simulation is performed to demonstrate the effectiveness of our technique for decenter sensing. We adopt a two-belts configuration as the simulated sparse aperture system, which consists of one sub-aperture in the center surrounded by other six sub-apertures. Each sub-aperture has a diameter of 2 mm and the baseline distances between two adjacent sub-apertures are assigned randomly. To show the attractive performance of our method for decenter sensing, two different array configurations are simulated corresponding to a sparse configuration and a compact one in order to test the convolution influence mentioned in eq. (3). To match closely with the experimental devices in our laboratory, we choose the following simulation parameters: 100 mm focal length of the converging lens, 1.67 μm pixel pitch of the CCD. To improve the facticity of the simulation, Gaussian noises are introduced to each intensity image captured by the detector. What is more, two kinds of errors are added to the simulation. The first error is the piston errors of the sub-apertures, and the other one is the modulating errors, generated by the phase-shift device.

Firstly, a sparse configuration is adopted for our simulation, which is shown in Fig. 2(a). In this image, the central No. 1 sub-aperture is regarded as the phase shifter. The piston errors of the sub-apertures are assigned randomly as shown in Fig. 2(b), whose values are ranging from −160 to 180 nm. Note that the added phase modulating error is 3 nm. We choose the right No. 2 sub-aperture as the tested aperture and other sub-apertures are the controls. To quantitatively introduce decenter, the tested sub-aperture has been moved in one direction with a spacing of 29.94 μm twenty times. At every position, four interference images are captured with different phase modulations by the phase shifter. After synthesizing these intensity images, the reconstructed

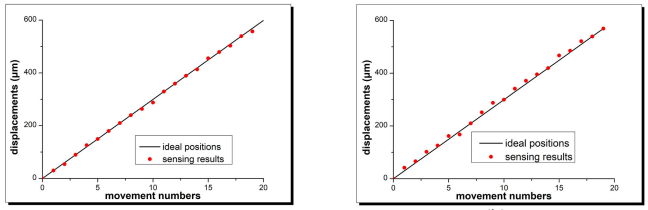

Fig. 3. The sensing result of the simulation. (a) The sparse configuration. (b) The compact configuration.

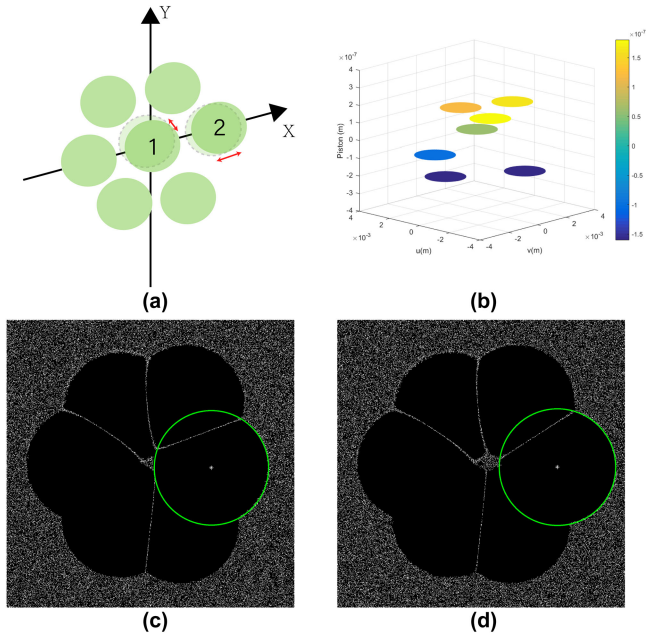

Fig. 4. Simulation setup of a compact configuration. (a) The seven apertures configuration. Aperture 1 produces phase shifts and aperture 2 produces decenters. (b) The loaded piston errors [−100∼180] nm. (c) The sensing results of Hough transform algorithm at initial position (the target aperture is with green circle). (d) The sensing results of Hough transform algorithm at final position (the target aperture is with green circle).

centering distributions are shown as Fig. 2(c) and Fig. 2(d), which correspond to the initial and the final positions, respectively. Apparently, the reconstructed tested sub-aperture (with a green circle) has a severe decenter error. The numerical values of the sensing result of the tested sub-aperture are presented in Fig. 3(a), from which we can find that the sensing positions almost exactly match the ideal position line. Note that in the twenty times movements, the sensing error is less than one pixel, which is acceptable in real system and proves the effectiveness of decenter sensing algorithm. The high sensing accuracy proves that the technique for decenter sensing has achieved the required performance and has great repeatability. In addition, it can be found that we can sense the decenters of all of the sub-apertures simultaneously.

The operation of utilizing the sub-aperture as the phase shifter causes the expansions of the reconstructed pupils, which leads to the pupils' overlap. Even so, we can still extract the decenters with our method. To present this attractive feature, corresponding simulation is also performed with a more compact configuration of telescope arrays shown as Fig. 4(a). Also, different piston errors are added to the telescope arrays, as presented in Fig. 4(b). Then, the No. 1 sub-aperture is used to generate phase modulations and the No. 2 sub-aperture is tested and introduced decenters with a spacing of 29.94 μm. The reconstructed centering distributions of the initial and final positions are

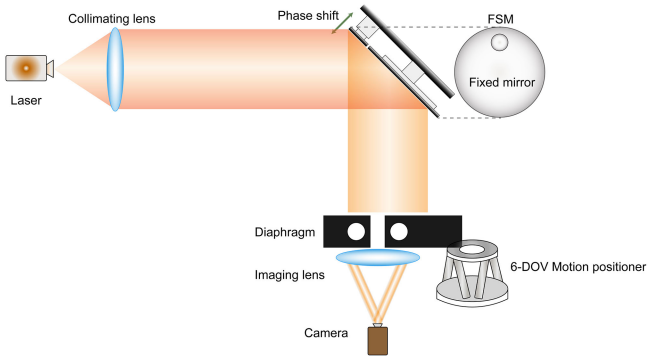

Fig. 5. The optical configuration of sparse apertures testbed. The FSM (the upper right), is composed of a small FSM segment and a fixed flat mirror segment. The 6-DOV (H-850, PI' product) platform can reach a spatial resolution of 0.3 μm.

shown in Fig. 4(c) and Fig. 4(d), respectively. It is easy to recognize that the reconstructed pupils are overlapped heavily. However, based on the limited boundaries of the overlapped pupil, we can still sense the decenter of the tested sub-aperture. The numerical values of the sensing result of the tested sub-aperture are presented in Fig. 3(b). It demonstrates that most residual errors are less than three pixels, which proves a fact that our approach is feasible not only in a sparse condition, but also in a compact arrays system.

4. Experimental Description and Results

So far, a method to evaluate decenter error in the sparse aperture telescope was studied. In this section, we have established a sparse aperture telescope testbed in our laboratory. In particular, we simply use the diaphragm to simulate the sparse aperture telescope. Fig. 5 shows the schematic of the optical components of the testbed and how the decenter for a sub-aperture is introduced. The wavelength of the laser is 632.8 nm. A collimator with a focal length of 3000 mm is used here as a scene projector. To generate the interference images of modulations, a phase generator is designed and built as shown at the upper right of Fig. 4, consisting of a small circular fast-steering mirror (FSM) surrounded by a fixed flat mirror. The accuracy of the FSM is less than 3 nm. Based on this structure, the phase modulations are added by moving the FSM along the axis direction. Note that the sparse aperture telescope is simulated by the combination of two diaphragms of which the diaphragm with one sub-aperture is actuated to introduce the decenter by a motion positioner (Hexapod H-850, PI' product) while the other is fixed on the experiment table to let the modulated beam pass through. Based on this structure, the decenter error is the dominant effect over any aberrations of the sparse aperture system. Moreover, the imaging lens with a focal length of 180 mm synthesizes the beams transmitted by those sub-apertures onto a CCD camera (Daheng Image's product, MER-1070-10GM/GC) with a 3840 $\times$ 2748 array of 1.67 μm pixel pitch.

After introducing the experimental setup, we present the sensing results. In this section, the configuration of two and three sub-apertures is performed to testify the effectiveness of our method. To start with, two sub-apertures with a diameter of 10 mm have been used as the simulated telescope to test. They are arranged horizontally in a center-to-center distance of 12 mm. In this configuration, one sub-aperture is regarded as the phase shifter while the other is taken as the decentered sub-aperture. Four interference images, shown in Fig. 6, are formed sequentially with an equivalent optical path difference (OPD) of 0.112 μm (equal to $\lambda/4\sqrt{2}$ by considering the reflection by the FSM). Note that these PSFs exhibit a high contrast and clear fringes with side lobes distributed symmetrically, which means the phase modulation generated by the FSM is of great accuracy. Then, the reconstructed centering distribution is obtained using the reconstruction algorithm, which is presented in Fig. 7(a). From the result we can find that the boundary of

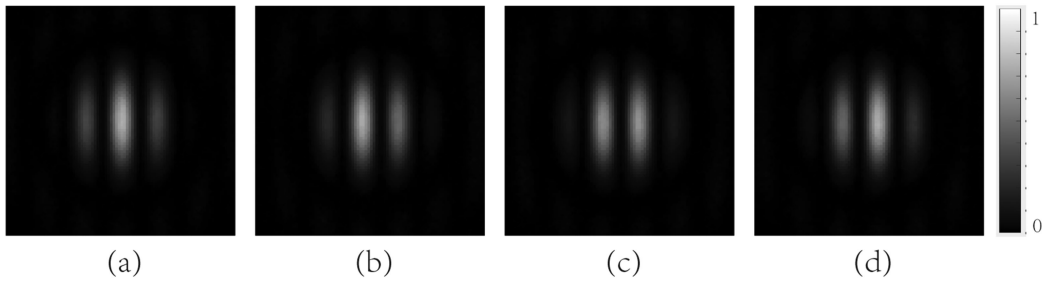

Fig. 6. Experimental modulation PSFs of two apertures system. (a)∼(d) are the PSFs corresponding to the phase modulations{Φ1;Φ2;Φ3;Φ4} = {0; $\pi/2$; π; $3\pi/2$}.

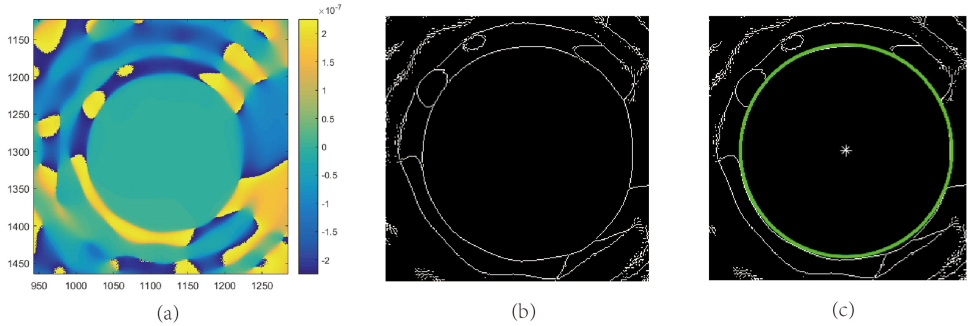

Fig. 7. Reconstructed image in two apertures system. (a) The image of reconstructed pupil distribution. (b) The binarization process result. (c) The sensing result with Hough Transform algorithm.

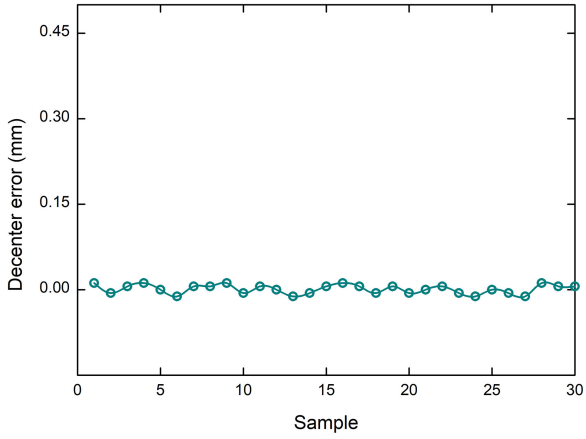

Fig. 8. Sensing results of decenter error in two sub-apertures testbed.

reconstructed pupil is perfectly clear and distinguishable, proving that it is feasible to discriminate the decenter of the tested sub-aperture. Consequently, the Fig. 7(b) is the binary picture of Fig. 7(a), and 7(c) is the sensing result of decenter. The absence of other positioning sensors in our lab limits us to verify the sensing accuracy directly. Thus, to test the accuracy of our method for decenter sensing we have moved the tested sub-aperture to introduce decenters quantitatively with an interval of 0.294 mm using a motion positioner, and repeated the test for three times to avoid the influence of accidental errors and other uncertain factors. All of the residual errors of decenters are presented in Fig. 8. It is noted that all of the residual differences are less than 0.0587 mm, which represents that our method for decenter sensing can realize an accuracy less than 1 pixel. The

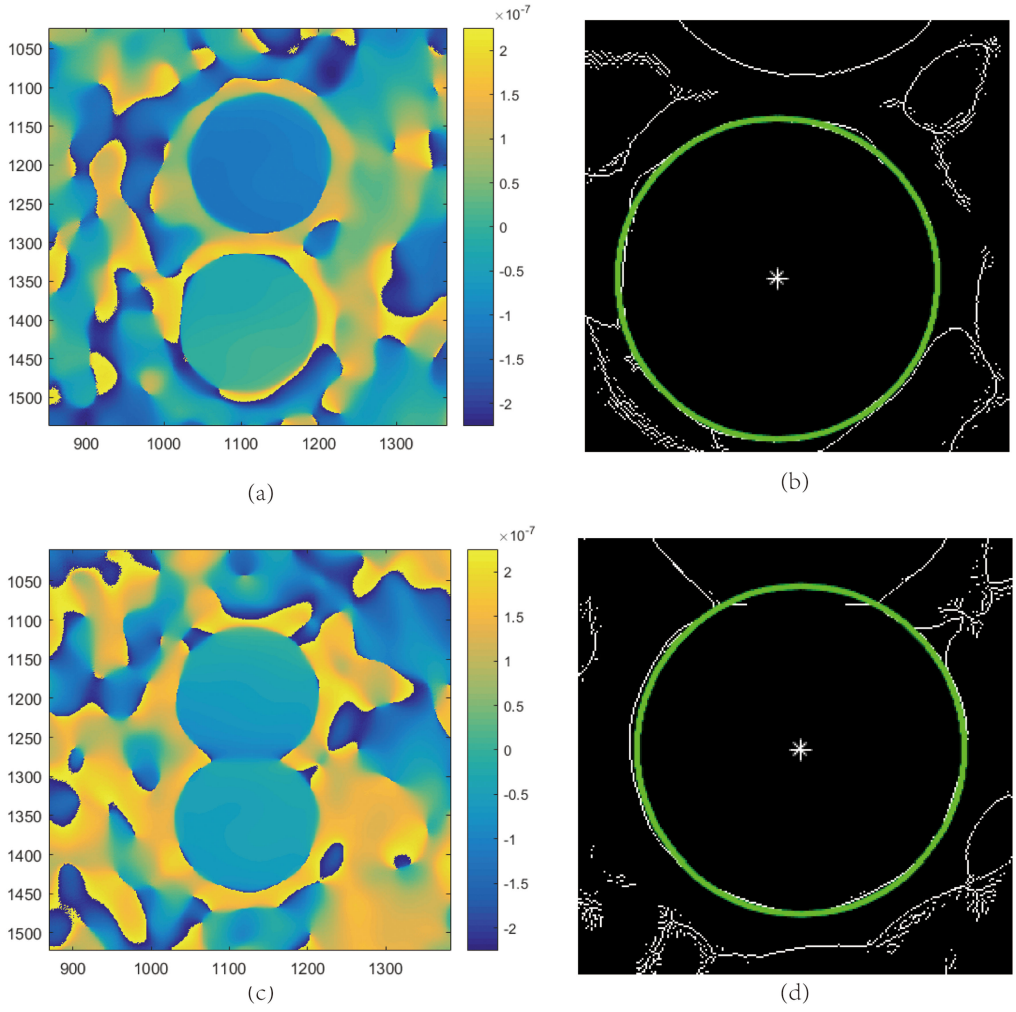

Fig. 9. Reconstructed image in three sub-apertures system. (a) and (c) are the images of reconstructed image in the initial and end positions. (b) and (d) are the sensing results of decenters with Hough Transform algorithm.

sensing results demonstrate that our algorithm for decenter sensing is accurate and the telescope apertures can be corrected within dozens of microns range based on our current experimental testbed. Furthermore, sub-pixel accuracy will be studied in the following work.

Then, we have tested the sensing performance in a three sub-apertures system to prove the effectiveness when the sub-apertures are arranged compactly. In this configuration, one sub-aperture is assigned as the phase shifter, the second one is introduced the decenter, and the last one is used as control. In the beginning, the baseline between two tested sub-apertures is long versus their diameters. Its reconstruction image is presented in Fig. 9(a), and the sensing result is shown in Fig. 9(b). Then we have moved the lower sub-aperture towards the upper one, and its reconstruction image is presented in Fig. 9(c). The decreased distance between the tested sub-apertures causes pupils' overlap, yet the boundaries of each tested sub-aperture are still distinguishable. Thus, the decenter is able to be acquired and the sensing result is shown in Fig. 9(d). The sensing accuracy is less than 3 pixels when the reconstructed pupils are overlapped, which is less than the accuracy for un-overlapped pupils.

In this section, the technology for decenter sensing succeeds in the sparse aperture telescope systems, and in turn the experimental results prove its high sensing performance. This method

works for not only the sparse apertures conditions, but also the more compact one, indicating that its capacity is robust to different conditions. There are two attractive advantages that have to be noted. On the one hand, we can obtain the decenter information of all of the sub-apertures simultaneously. On the other hand, the other WFE information like piston and tip-tilt is also acquired.

5. Conclusion

To conclude, a new method has been proposed and demonstrated for the decenter sensing with a phase shift and centroid extraction algorithm in the sparse aperture systems. This method is, to the best of our knowledge, the first one to measure the decenter error without adding any extra sensors. It can measure not only the decenter, but also the piston and tip-tilt at the same time. Firstly, simulations of seven sub-apertures are performed to validate the decenter sensing performance under the condition of background noise and phase modulating error. The decenter sensing results show that the measurements can be done not only in the sparse aperture systems but also in the compact condition. Then, an appropriate experimental testbed is built to test the performance in real system. The decenter sensing accuracy on the two sub-apertures system with real images is less than 1 pixel, which shares a similar value to that on simulation, further demonstrating the effectiveness of decenter sensing. The experimental result of three-aperture system demonstrates that our method can also be applied to sense the decenter when the reconstructed pupils are overlapped. The high accuracies in both simulations and experiments indicate that our method for decenter sensing is promising owing to the needlessness of installing any additional sensor and applicability to both sparse and compact configuration, which we believe will be widely applied in sparse aperture arrays.

References

[1] M. Clampin, "Status of the James Webb space telescope observatory," *Proc. SPIE*, vol. 8442, 2012, Art. no. 84422A.
[2] R. Gilmozzi and J. Spyromilio, "The 42m european ELT: Status," *Proc. SPIE*, vol. 7012, 2008, Art. no. 701219.
[3] R. L. Kendrick *et al.*, "Wide-field Fizeau imaging telescope: Experimental results," *Appl. Opt.*, vol. 45, no. 18, pp. 4235–4240, 2006.
[4] M. Faucherre, F. Merkle, and F. Vakili. "Beam combination in aperture synthesis from space: Field of view limitations and (U,V) plane coverage optimization," *Proc. SPIE*, vol. 1130, 1989, Art. no. 138145.
[5] C. R. D. Hainaut, K. P. Hentz, L. D. Weaver, and J. D. Gonglewski, "Design of a wide field of view phased array telescope," *Opt. Eng.*, vol. 27, no. 9, pp. 736–739, 1988.
[6] S.-J. Chung, "Design, implementation and control of a sparse aperture imaging satellite," M.S. thesis, Dept. Aeronaut. Astronaut., MIT, Cambridge, MA, USA, 2002.
[7] J. E. Harvey and C. Ftaclas, "Field-of-view limitations of phased telescope arrays," *Appl. Opt.*, vol. 34, no. 25, pp. 5787–5798, 1995.
[8] G. Chanan *et al.*, "Phasing the mirror segments of the Keck telescopes: The broadband phasing algorithm," *Appl. Opt.*, vol. 37, no. 1, pp. 140–155, 1998.
[9] G. Chanan, C. Ohara, and M. Troy, "Phasing the mirror segments of the Keck telescopes II: The narrow-band phasing algorithm," *Appl. Opt.*, vol. 39, no. 25, pp. 4706–4714, 2000.
[10] S. Esposito, E. Pinna, A. Puglisi, A. Tozzi, and P. Stefanini, "Pyramid sensor for segmented mirror alignment," *Opt. Lett.*, vol. 30, no. 19, pp. 2572–2574, 2005.
[11] M. A. van Dam, B. A. McLeod, and A. H. Bouchez, "Dispersed fringe sensor for the giant magellan telescope," *Appl. Opt.*, vol. 55, no. 3, pp. 539–547, 2016.
[12] F. Shi *et al.*, "Segmented mirror coarse phasing with a dispersed fringe sensor: Experiment on NGST's wavefront control testbed," *Proc. SPIE*, vol. 4850, 2003, doi: 10.1117/12.461113.
[13] S. Chris and L. C. Roberts Jr., "How to calibrate edge sensors on segmented mirror telescopes," *Proc. SPIE*, vol. 8444, 2012, Art. no. 844460.
[14] J. Nelson and G. H. Sanders, "The status of the thirty meter telescope project," *Proc. SPIE*, vol. 7012, 2008, Art. no. 70121A.
[15] M. Johns, "Progress on the GMT," *Proc. SPIE*, vol. 7012, 2008, Art. no. 70121B.
[16] F. Hénault, "Conceptual design of a phase shifting telescope-interferometer," *Opt. Commun.*, vol. 261, pp. 34–42, 2006.
[17] F. Hénault, "Analysis of stellar interferometers as wavefronts sensors," *Appl. Opt.*, vol. 44, pp. 4733–4744, 2005.
[18] F. Hénault, "Multi-spectral piston sensor for co-phasing giant segmented mirrors and multi-aperture interferometric arrays," *J. Opt.: Pure Appl. Opt.*, vol. 11, no. 12, 2009, Art. no. 125503.
[19] P. V. C. Hough. "A method and means for recognizing complex patterns," US Patent 3,069,654, Dec. 18, 1962.
[20] D. H. Ballard, "Generalizing the hough transform to detect arbitrary shapes," *Pattern Recognit.*, vol. 13, no. 2, pp. 111–122, 1981.
[21] S. Maji and J. Malik, "Object detection using a max-margin hough transform," in *Proc. IEEE Conf. Comput. Vis. Pattern Recognit.*, 2009, pp. 1038–1045.